Interaction of Bismuth Oxide Cluster Cations with Alkenes and Molecular Oxygen: $Bi_4O_6^+$, a Possible Reactive Center for Alkene Oxidation

André Fielicke and Klaus Rademann*

Walther-Nernst-Institut für Physikalische und Theoretische Chemie der Humboldt-Universität zu Berlin, Bunsenstrasse 1, D-10117 Berlin, Germany

Received: March 31, 2000

The activation of molecular oxygen by bismuth oxide cluster cations has been observed in the presence of unsaturated hydrocarbon molecules. Reactivities of gas-phase bismuth oxide cluster cations $Bi_xO_y^+$ ($x = 3$ or 4, $y \leq 7$) with hydrocarbons have been studied by measuring scattering cross sections and analyzing products formed under multiple collision conditions. The integral cross sections for the scattering of the cations $Bi_xO_y^+$ ($x = 3$ or 4, $y \leq 7$) from argon, alkanes (methane, propane, butane), and alkenes (ethene, propene, 1-butene, 1,3-butadiene) have been measured. In particular, the cation $Bi_4O_6^+$ has a significantly increased cross section for the scattering from the alkenes as compared to the other oxides $Bi_4O_y^+$. The larger total cross section is explained by assuming an increased cross section for reactive collisions, which could be caused by a specific reactivity of that cation. Products for the reactions of small bismuth oxide cluster cations $Bi_xO_y^+$ ($x = 3$ or 4) with ethene and propene have been investigated by conducting fast-flow reactor experiments. In the series $Bi_xO_y^+$ ($x = 3$ or 4), a simple addition of one or more alkene molecules to the oxide cation has been observed. Only $Bi_4O_6^+$ is special, because it shows addition of alkene *and* O_2 as shown by the formation of Bi_4O_8-(alkene)$^+$ and Bi_4O_8(alkene)$_2^+$.

Introduction

The oxidation of alkenes on metal oxide and transition metal oxide catalysts is an industrial process of great importance. Various oxygenators are being used, but difficulties occur for the obvious oxidant molecular oxygen concerning activation and selectivity of the oxidation. The link between reactivity and selectivity is the key to improving catalytic alkene oxidation.[1−3] Catalysts containing bismuth oxide compounds are used for instance for the production of acrylonitrile and acrolein by oxidation or ammoxidation of propene,[4] but the mechanisms on a molecular level are not completely known. This is not surprising, as real catalysts are generally multicomponent systems. For instance, Bi, Mo, P, Si, O, and other elements are ingredients of the catalysts in the exemplary propene oxidation. However, investigations of binary bismuth oxide clusters could be helpful for better understanding details of oxygen transfer reactions. Metal oxide clusters are suitable model systems for studying reactive sites in heterogeneous oxidation reactions.[5−9] Moreover, ab initio computational chemistry methods are accessible for determining the cluster structural and energetic properties, which are needed for the interpretation of experimental findings.

Recent research on bismuth oxide clusters has been mainly concerned with stoichiometric and closed shell oxides $(Bi_2O_3)_n$ and cations $(Bi_2O_3)_nBiO^+$. Cluster beams produced by employing reactive laser vaporization,[10] gas aggregation,[11−13] arc discharge,[14] or ^{252}Cf sputtering[15] sources contain these oxide clusters in large amounts, indicating their special stability. The stability is also supported by model calculations.[10,12] For example, ground state structure calculations yield compact cage structures, which are regularly built up from 2-fold coordinated oxygen and 3-fold coordinated bismuth. In the case of cationic clusters the charge could be located at 3-fold coordinated O or 2-fold coordinated Bi.[12] Hence, the constituents assume their most stable oxidation states, −2 for O and +3 for Bi. These building principles are in line with the structures of the corresponding oxide clusters of antimony.[16,17] Sb_4O_6 and Bi_4O_6 have geometries similar to the well-known structures of other stable gas-phase oxides of group V such as P_4O_6 or As_4O_6.[18] Generally, the knowledge of cluster structures is crucial for understanding intrinsic cluster reactivities.

Recent experiments on the scattering of bismuth oxide clusters $(Bi_2O_3)_nBiO^+$ ($1 \leq n \leq 4$) by ethene and propene have shown that these oxides exhibit a stronger depletion than the analogous antimony oxide clusters.[12,13] This result has been interpreted in terms of an increased reactivity of the bismuth oxide clusters. The observation that bismuth oxide clusters are reactive is in line with the fact that alkenes react readily with bulk Bi_2O_3, while the solid antimony(III) oxide does not react. Reactivities for oxide cations other than the intense and stable closed shell $(Bi_2O_3)_nBiO^+$ have not been studied up to now. Bienati, Bonačić-Koutecký, and Fantucci have investigated most recently the interaction between bismuth oxide cations and alkenes as well as the effect of additional molecular oxygen and the possibility of the production of stable alkene−bismuth oxide adducts. This theoretical work is presented in the accompanying article in this issue.[19]

Here, we report experimental findings on reactivities of closed shell *and* radical bismuth oxide cations. The cross sections for the scattering of bismuth oxide cations from alkenes are particularly increased for $Bi_4O_6^+$. Also, the reaction products formed under multiple collision conditions indicate the special reactivity of this cation.

Experimental Section

The mass spectra have been measured in a three-stage molecular beam apparatus that will be briefly described in the

10.1021/jp001257m CCC: $19.00
Published on Web 07/07/2000

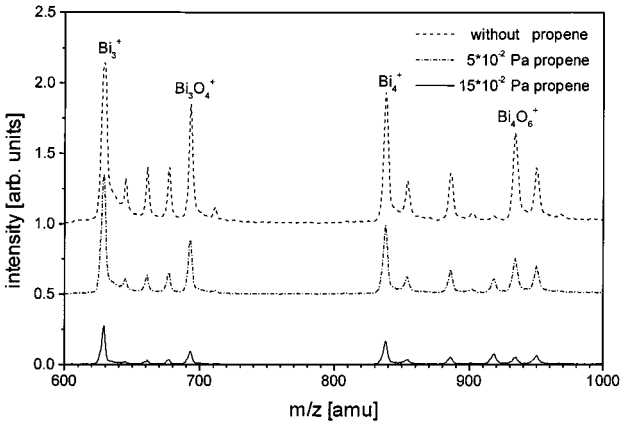

Figure 1. Mass spectra of cationic bismuth clusters and bismuth oxide clusters. By adding propene, the intensities are increasingly depleted due to collisions of the clusters in the scattering cell.

following. The apparatus consists of three components: a laser vaporization cluster source with an added reaction channel, an extra scattering cell for collision experiments, and a time-of-flight mass spectrometer. These components are mounted in differentially pumped vacuum chambers, which are separated by a skimmer and a 5 mm aperture, respectively.

The laser vaporization cluster source works with a continuous flow of carrier gas at room temperature. The design of the source with an attached reaction channel is similar to the known "fast-flow reactor" arrangements.[20,21] The reaction channel is assembled of separate segments with individual gas inlets, thus allowing the variation of the total passing time and the reaction time by modifying the channel length between 35 and 140 mm. The beam of a pulsed frequency doubled Nd:YAG laser (Continuum Powerlite 6030) is focused on a rotating bismuth rod. The produced plasma is carried through a channel of 4 mm inner diameter and 105 mm length by a continuous flow of usually 10% oxygen in helium. Because of the high oxygen content, the bismuth will be partly oxidized in the plasma, and after collisional cooling the oxide clusters are formed. These undergo reactions in the channel if hydrocarbons are added. The reactive gas entrance is located 40 mm before where the channel is narrowed to a 2-mm nozzle. A capacitance pressure sensor (MKS Baratron Type 626) is attached near the nozzle to measure the gas pressure in the channel. During the following expansion into a vacuum chamber a molecular beam containing cations, anions, and neutral species is formed and shaped by a skimmer (2 mm orifice). The beam passes the collision cell, which is located in a differentially pumped vacuum stage. The absolute gas pressure in the scattering cell is measured with a second Baratron sensor, which is connected directly to the cell by a 10 mm diameter tube. After having passed the scattering cell, the cluster beam enters the mass spectrometer chamber. The time-of-flight mass spectrometer is constructed as described by Wiley and McLaren[22] with a mass resolution of typically 300. The cations are accelerated perpendicular to the molecular beam by applying a pulsed electric field. An einzel lens and a set of deflector plates focus the ion beam onto a modified Daly-Detector ("Even-Cup").[23,24] The signals are amplified 16 times by a timing amplifier (EG&G Ortec 574) and recorded with a digital oscilloscope (LeCroy 9350CM). The data are transmitted to a personal computer, and the mass spectra are analyzed with the Microcal Origin (version 4.1) program.

Results and Discussion

Scattering Cross Sections. Figure 1 shows parts of typical mass spectra of bismuth oxide cations in the mass range of $Bi_3O_y^+$ and $Bi_4O_y^+$. The oxides are produced at a typical carrier gas pressure of 1500 Pa (10% O_2 in He) in the source channel. Intense peaks of the bare bismuth cluster cations are accompanied by oxide peaks. $Bi_3O_4^+$ is the most intense oxide, representing the high thermodynamic stability of this closed shell oxide cluster. In the $Bi_4O_y^+$ range no stoichiometric oxide cation with all bismuth atoms in +3 and oxygen in −2 oxidation stage exists. The radical character of $Bi_4O_6^+$ might cause changes in reactivity, as will be shown by further analysis. Note that the signals for the oxide cations $Bi_4O_y^+$ with $y = 2$, 4 or 5 are very weak or absent. All signals are depleted, if hydrocarbons are introduced in the scattering cell.

To derive scattering cross sections, the peak intensities in these mass spectra are integrated and fitted to the given exponential law

$$I = I_0 e^{-\sigma n_B L}$$

where I is the measured integrated peak intensity, I_0 is the calculated intensity without scattering gas, σ is the scattering cross section for a given cluster, n_B is the particle density of the scattering gas, and L (=100 mm) is the length of the collision zone. Only cluster cations, which appear abundant enough at further depletion, have been evaluated. Our experimental method measures the depletion in the direction of the molecular beam. Therefore the derived scattering cross sections are integral or total, not angularly resolved quantities. These cross sections are determined for the alkanes methane, propane, and butane, the alkenes ethene, propene, 1-butene, 1,3-butadiene, and also for argon between 1×10^{-2} and 3×10^{-1} Pa in the collision cell at room temperature (25 °C). By employing the hard-sphere model, we estimate the number of collisions of a single cluster to be in the range of typically less than 10. The cations are not accelerated; their kinetic energy is defined by the velocity of the molecular beam (about 1000 m s^{-1}). Figure 2 shows the cross sections for bismuth and bismuth oxide clusters $Bi_3O_y^+$ ($0 \le y \le 4$) and $Bi_4O_y^+$ ($y = 0$, 1, 3, 6, or 7). The given values are not corrected for the geometry of the scattering zone and the detector. Because of our experimental setup, also particles, which are deflected under small angles to the beam axis, can reach the entrance slit of the mass spectrometer. A simple evaluation of the cross sections for cluster ion−molecule interactions can be given by the Langevin model.[25] For $Bi_4O_6^+$ with a velocity of 1000 m s^{-1} and ethene, this cross section has been calculated to be 15.8 Å^2. The determined experimental value is higher, certainly due to the contributing gas kinetic cross section and multiple collision effects. In the following, we discuss the dependencies of our experimental cross sections as effective quantities without further corrections.

The cross sections generally increase with molecular size of the hydrocarbons. This observation can be explained partly by elastic interactions but also by increasing inelastic and reactive interactions due to growing polarization effects, which become important in the case of cluster cations. The scattering cross sections are distinctly larger for alkenes than for the alkanes with the same number of C-atoms, because of the stronger nucleophility of the alkenes. For all cations, Bi_3^+ and the series $Bi_3O_y^+$, the cross sections for a given scattering gas are nearly identical (Figure 2a). For methane, for instance, this can be understood in terms of ion−induced dipole interactions. With regard to Bi_4^+ and $Bi_4O_y^+$, the scattering cross sections are also very similar for a given scattering gas; only $Bi_4O_6^+$ differs characteristically (Figure 2b). The scattering cross sections for the systems $Bi_4O_6^+$−alkenes are significantly increased by about

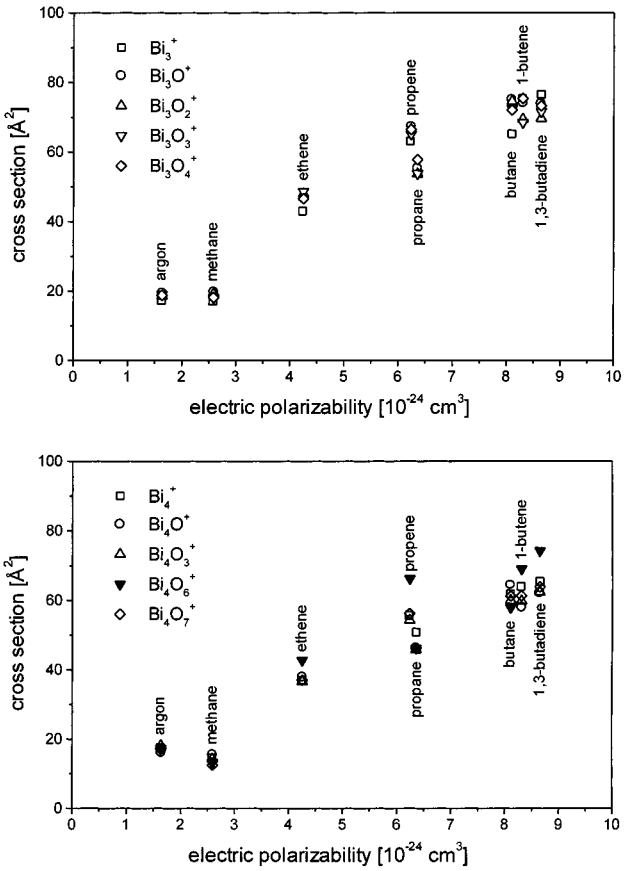

Figure 2. Integral cross sections for the scattering of cluster cations $Bi_3O_y^+$ (a, top) and $Bi_4O_y^+$ (b, bottom) with hydrocarbons and argon. The average static electric polarizabilities[27] were chosen to characterize the hydrocarbons. Argon was selected to refer to the concomitant nonreactive scattering.

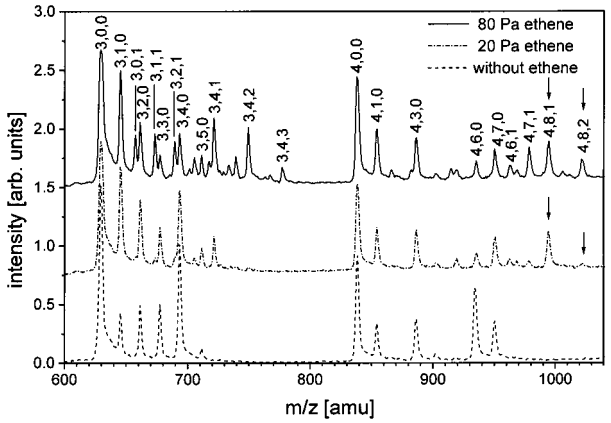

Figure 3. Abundance spectra of cationic bismuth clusters, bismuth oxide clusters, and reaction products. The products are formed under multiple collision conditions in the "fast flow reactor", when ethene is added. The compositions for the cluster cations $Bi_xO_y(C_2H_4)_z^+$ are written as triples *x*,*y*,*z*. The peaks derived from $Bi_4O_6^+$ by picking up ethene and oxygen are marked with arrows.

SCHEME 1: Experimentally Determined Pathways for Product Formation

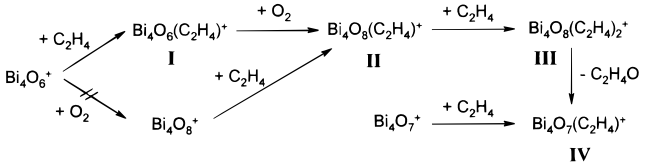

20% with respect to the other oxides $Bi_4O_y^+$. As the clusters and the hydrocarbons have many internal degrees of freedom, it is reasonable to assume that the collisions are rather inelastic or reactive than elastic. The increased total cross section of $Bi_4O_y^+$ might be due to different processes: collision induced fragmentation, electron transfer, or chemical reactions. Fragmentations should be excluded, as we can expect a similar fragmentational behavior for alkanes and alkenes, which has not been observed. Because of the high ionization potential of the alkenes (around 10 eV), electron capture by $Bi_4O_6^+$ is rather improbable. Therefore, we suppose that especially $Bi_4O_6^+$ reacts readily with alkenes, possibly leading to the production of adducts. In fact, the formation of adducts is in agreement with theory.[19]

Product Formation. Compositions of reaction products for the multiple collision flow tube experiments are derived from product mass spectra as shown in Figure 3. Ethene was introduced into the reaction channel with typical pressures of about 100 Pa. The distance between the gas inlet and the nozzle is 40 mm. The product distributions have been measured at room temperature (ca. 25 °C). The distance between the spot of vaporization and the reactive gas inlet is always 65 mm. If this distance is increased to 110 mm, the absolute cluster and product intensity is decreased as expected. However, the relative abundance distributions of the products remain nearly unchanged. Therefore, we assume that the clusters are thermalized at the reactive gas inlet position at 65 mm.

The product distributions for $Bi_xO_y(C_2H_4)_z$ differ characteristically for $x = 3$ and $x = 4$. As for $Bi_3O_y^+$, adducts with one or more ethene molecules have been detected. Adducts deriving from $Bi_3O_4^+$ are most intense. Since the sum of the intensities of all cations $Bi_3O_4(C_2H_4)_z^+$ ($0 \le z \le 3$) is nearly constant, we assume that these products are formed by successive addition of ethene to $Bi_3O_4^+$. The increasing intensities of the clusters Bi_3O^+ and $Bi_3O_2^+$ seem to be caused by reductive fragmentation of larger clusters, induced by the alkene. The $Bi_4O_y^+$ region is dominated by peaks, which have no analogues in the $Bi_3O_y^+$ range. At low ethene partial pressure the $Bi_4O_6^+$ signal is depleted and a peak appears, which could be assigned to $Bi_4O_8(C_2H_4)^+$. By further adding ethene, new signals for $Bi_4O_8(C_2H_4)_2^+$ and $Bi_4O_7(C_2H_4)^+$ occur. The sum of the intensities of the four last mentioned clusters is nearly constant. We conclude that $Bi_4O_8(C_2H_4)^+$ and $Bi_4O_8(C_2H_4)_2^+$ are produced by consecutive addition of ethene and molecular oxygen that is part of the carrier gas.

The specific reactivity of $Bi_4O_6^+$ is very different to that of the $Bi_3O_y^+$ and $Bi_2O_y^+$ clusters, since $Bi_3O_y^+$ and $Bi_2O_y^+$ cations only show ethene adducts and never subsequential oxygenation. In the following, we discuss several suggestions on the reaction mechanisms starting with $Bi_4O_6^+$. These proposals are summarized in Scheme 1. The addition of ethene to $Bi_4O_6^+$ leads to the formation of the reactive intermediate $Bi_4O_6(C_2H_4)^+$ (**I**) which readily adds molecular oxygen and forms $Bi_4O_8(C_2H_4)^+$ (**II**). The alternative sequence with intermediate formation of $Bi_4O_8^+$ seems to be improbable: $Bi_4O_8^+$ does not appear in the mass spectra and theoretical calculations yield that $Bi_4O_8^+$ is not stable. Examination of the scattering from O_2 also yields no special interaction between $Bi_4O_6^+$ and molecular oxygen. Therefore, we assume that the association of $Bi_4O_6^+$ and ethene is the first step and the addition of O_2 is the second step in the formation of $Bi_4O_8(C_2H_4)^+$ (**II**). Theoretical investigations strongly support this assumption, since $Bi_4O_6^+$ has been identified as a radical species with an unpaired electron located at one of the bridging oxygen atoms which induces the high

reactivity of this species with alkenes. The structure of the intermediate **I** has been calculated as a Bi_4O_6 cage with added C_2H_4, bound to an oxygen atom (see ref 19 Figure 8, structure b). In **I** the spin is located at the outer C-atom, which reacts with molecular oxygen leading to the formation of the alkyl superoxide radical $Bi_4O_6^+C_2H_4O_2^\bullet$ (**II**). Superoxides are often-discussed intermediates in oxidation, combustion processes, and atmospheric chemistry, where alkyl radicals are involved.[26] Further addition of one ethene molecule to **II** yields the peroxide $Bi_4O_6^+C_2H_4OOC_2H_4^\bullet$ (**III**). The species $Bi_4O_7(C_2H_4)^+$ (**IV**) probably originates from **III** by releasing a neutral oxidation product C_2H_4O. A small amount of **IV** could be formed by direct alkene addition to $Bi_4O_7^+$, but the intensity of $Bi_4O_7^+$ decreases only slightly by increasing the alkene partial pressure. Details of this reaction mechanism including structures of the involved compounds and energetics computed with DFT methods are presented in the accompanying article.[19] The same sequence of reaction steps has also been observed for propene, but the adduct intensities of the latter are stronger at the same partial pressure of the alkene. As discussed above, the higher reactivity corresponds to the larger scattering cross sections for the systems $Bi_xO_y^+$−propene.

The interaction of $Bi_4O_6^+$ with alkenes shows a distinct reactivity as demonstrated by the increased cross sections and the product distributions. This behavior is probably due to a specific electronic and geometric structure. In this context, it is of interest to emphasize the properties found for the homologous series $(Bi_2O_3)_n^+$. The first element $Bi_2O_3^+$ ($n = 1$) exhibits only addition of alkene, in contrast to $Bi_4O_6^+$ ($n = 2$) and $Bi_6O_9^+$ ($n = 3$), for which the addition of alkene and extra addition of molecular oxygen has been found. Also, all radicals in the $(Bi_2O_3)_n^+$ series (with $n = 2$, 3, or 4) exhibit increased scattering cross sections. We suggest that this size-dependent onset of special reactivity could be explained in terms of new structural patterns, which appear first in the $Bi_4O_6^+$ structure. This structural element has been identified as bridging oxygen with localized electron spin as discussed in the accompanying theoretical article.[19]

Conclusion

We observe a distinct reactivity of $Bi_4O_6^+$ with alkenes, which is reflected by increased scattering cross sections, and also by different product distributions. We explain the production mechanism for the complex $Bi_4O_8(C_2H_4)^+$ by successive addition of ethene and molecular oxygen to $Bi_4O_6^+$. On the basis of this special behavior, we suppose $Bi_4O_6^+$ to be a possible reactive center for the activation of molecular oxygen and oxidation of alkenes. The detection of $Bi_4O_7(\text{alkene})^+$ indicates the formation of alkene oxidation products with sum formulas C_2H_4O for ethene and C_3H_6O for propene. Further investigations should be directed to the oxygen transfer toward the alkene and the product formation, which could possibly be done by ion cyclotron resonance mass spectrometry methods.

Acknowledgment. We gratefully acknowledge support by the Deutsche Forschungsgemeinschaft, the Fonds der Chemischen Industrie, and the Humboldt-Forschungs Fonds.

References and Notes

(1) Kung, H. H. *Transition metal oxides: surface chemistry and catalysis*; Elsevier: Amsterdam, 1989.
(2) *New Developments in Selective Oxidation*; Centi, G., Triffiró, F., Eds.; Elsevier: Amsterdam, 1990.
(3) *New Developments in Selective Oxidation II*; Corberán, V. C., Bellón, S. V., Eds.; Elsevier: Amsterdam, 1994.
(4) *Ullmann's Encyclopedia of Industrial Chemistry, Electronic Release*, 6th ed.; Wiley-VCH: Weinheim, 1998.
(5) Deng, H. T.; Kerns, K. P.; Castleman, A. W., Jr. *J. Phys. Chem.* **1996**, *100*, 13386−13392.
(6) Fialko, E. F.; Kikhtenko, A. V.; Goncharov, V. B.; Zamaraev, K. I. *J. Phys. Chem. A* **1997**, *101*, 8607−8613.
(7) Koretsky, G. M.; Knickelbein, M. B. *J. Chem. Phys.* **1997**, *107*, 10555−10566.
(8) Bell, R. C.; Zemski, K. A.; Kerns, K. P.; Deng, H. T.; Castleman, A. W., Jr. *J. Phys. Chem. A* **1998**, *102*, 1733−1742.
(9) Zemski, K. A.; Bell, R. C.; Castleman, A. W., Jr. *Int. J. Mass Spectrom.* **1999**, *184*, 119−128.
(10) France, M. R.; Buchanan, J. W.; Robinson, J. C.; Pullins, S. H.; King, R. B.; Tucker, J. L.; Duncan, M. A. *J. Phys. Chem. A* **1997**, *101*, 6214−6221.
(11) Kinne, M.; Bernhardt, T. M.; Kaiser, B.; Rademann, K. *Int. J. Mass Spectrom. Ion Processes* **1997**, *167/168*, 161−172.
(12) Kinne, M.; Heidenreich, A.; Rademann, K. *Angew. Chem.* **1998**, *110*, 2637−2639.
(13) Kinne, M.; Rademann, K. *Chem. Phys. Lett.* **1998**, *284*, 363−368.
(14) Opitz, J.; Kaiser, B.; Rademann, K. Unpublished results.
(15) Van Stipdonk, M. J.; Justes, D. R.; English, R. D.; Schweikert, E. A. *J. Mass Spectrom.* **1999**, *34*, 677−683.
(16) Reddy, B. V.; Jena, P. *Chem. Phys. Lett.* **1998**, *288*, 253−260.
(17) Kaiser, B.; Bernhardt, T. M.; Kinne, M.; Rademann, K.; Heidenreich, A. *J. Chem. Phys.* **1999**, *110*, 1437−1449.
(18) Greenwood, N. N.; Earnshaw, A. In *Chemistry of the elements*; Pergamon Press: Oxford, 1994; pp 577, 668.
(19) Bienati, M.; Bonačić-Koutecký, V.; Fantucci, P. *J. Phys. Chem. A* **2000**, *104*, 6983.
(20) Geusic, M. E.; Morse, M. D.; O'Brien, S. C.; Smalley, R. E. *Rev. Sci. Instrum.* **1985**, *56*, 2123−2130.
(21) Richtsmeier, S. C.; Parks, E. K.; Liu, K.; Pobo, L. G.; Riley, S. J. *J. Chem. Phys.* **1985**, *82*, 3659−3665.
(22) Wiley, W. C.; McLaren, I. H. *Rev. Sci. Instrum.* **1955**, *26*, 1150−1157.
(23) Daly, N. R. *Rev. Sci. Instrum.* **1960**, *31*, 264−267.
(24) Bahatt, D.; Cheshnovski, O.; Even, U.; Lavie, N.; Magen, Y. *J. Phys. Chem.* **1987**, *91*, 2460−2462.
(25) Henchman, M. Rate Constants and Cross Sections. In *Ion−Molecule Reactions*; Franklin, J. L., Ed.; Plenum Press: New York, 1972; Vol. 1; pp 186−200.
(26) Chen, C.; Bozzelli, J. W. *J. Phys. Chem. A* **1999**, *103*, 9731−9769.
(27) *CRC Handbook of Chemistry and Physics*; CRC Press: Boca Raton, FL, 1995.